The Emerald Research Register for this journal is available at
http://www.emeraldinsight.com/researchregister

The current issue and full text archive of this journal is available at
http://www.emeraldinsight.com/0961-5539.htm

Received July 2002
Revised October 2002
Accepted January 2003

Modeling of cavitating or ventilated flows using BEM

Spyros A. Kinnas
Ocean Engineering Group, The University of Texas at Austin, Austin, Texas, USA

Yin L. Young
Department of Civil and Environmental Engineering, Princeton University, Princeton, New Jersey, USA

Keywords *Cavitation, Boundary elements methods, Hydrofoils*

Abstract *Boundary element method (BEM) techniques for the prediction of cavitating or ventilated flows around hydrofoils and propeller are summarized. Classical, supercavitating, and ventilated blade section geometries are considered. Recent extensions which allow for the modeling of cavities on either or both sides of the blade surface are presented. Numerical validation studies and comparisons with experimental measurements are shown.*

1. Introduction

Cavitation occurs when pressure drops below the saturated vapor pressure of the liquid, consequently resulting in the formation of gas filled or gas and vapor filled bubbles. A type of cavitation that is common on marine propulsors is *sheet* cavitation. It is characterized by a "continuous" liquid/vapor interface which is "attached" to the blade surface. Despite its undesirable nature, some sheet (or other types of) cavitation often has to be accepted in order to maintain efficiency. Thus, accurate prediction of cavitation is very crucial in the design and analysis of marine propulsors.

Another common phenomena for marine propulsors is ventilation, which occurs when surface air or exhaust gases are drawn into the lifting surface. Examples of different types of high-speed hydrofoils are shown in Figure 1. A photo of a supercavitating hydrofoil is shown in Figure 2. Note that in the case of a ventilated hydrofoil, ventilation is forced by continuously injecting air to the upper foil surface. In the case of a surface-piercing hydrofoil, ventilation is a result of air drawn from the free surface. In both cases, the objective is to increase the lift to drag ratio at high-speed operations. Note that the pressure in the ventilated surface is constant, but equal to a value that is different from the

Support for this research was provided by Phase III of the "Consortium on Cavitation Performance of High Speed Propulsors" with the following members: AB Volvo Penta, American Bureau of Shipping, El Pardo Model Basin, Hyundai Maritime Research Institute, Kamewa AB, Michigan Wheel Corporation, Naval Surface Warfare Center Carderock Division, Office of Naval Research (Contract N000140110225), Ulstein Propeller AS, VA Tech Escher Wyss GMBH, and W*ä*rtsil*ä* Propulsion.

International Journal of Numerical Methods for Heat & Fluid Flow
Vol. 13 No. 6, 2003
pp. 672-697
© MCB UP Limited
0961-5539
DOI 10.1108/09615530310498376

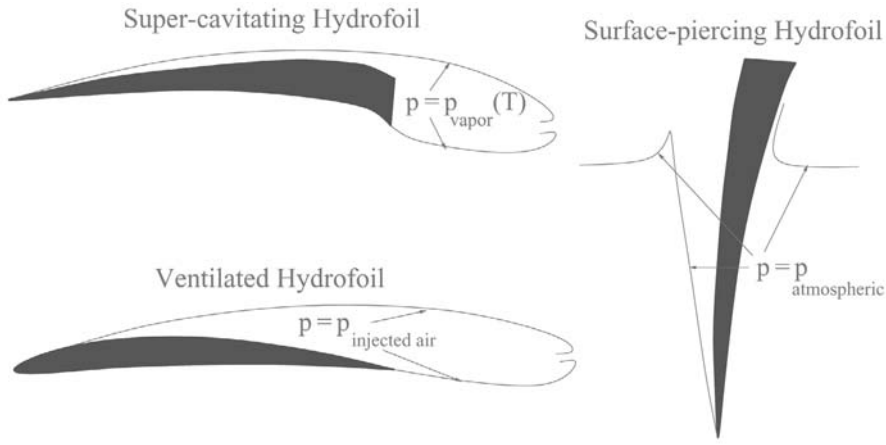

Figure 1.
Schematic of different types of high-speed hydrofoils (Kinnas *et al.*, 2001)

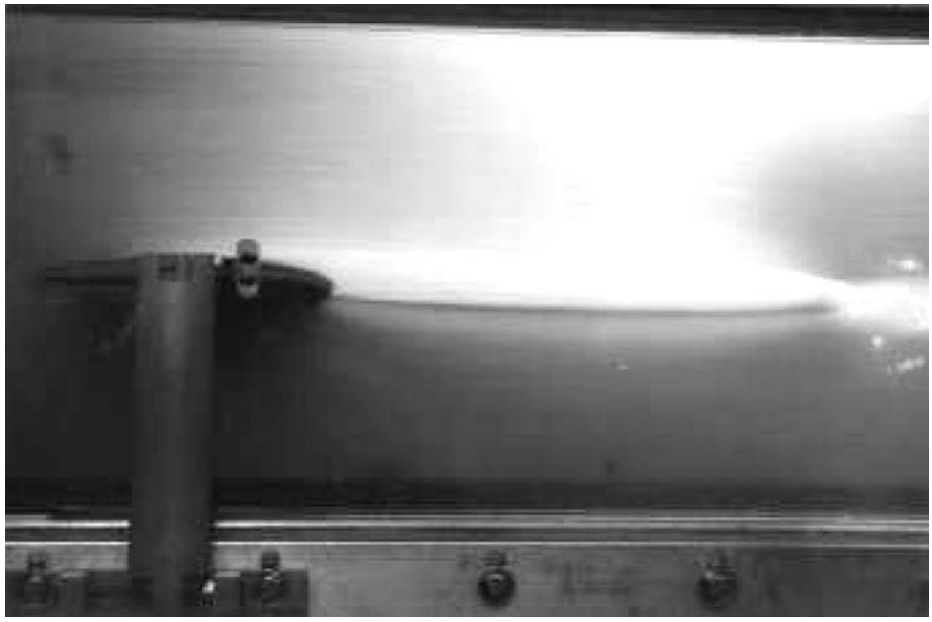

Figure 2.
Photo of a supercavitating hydrofoil experiment inside MIT's Marine Hydrodynamics Water Tunnel, $l/c \approx 3$ (Kinnas and Mazel, 1993)

vapor pressure. Thus, the ventilated cavity surface can be modeled like a sheet cavity surface with a different prescribed pressure.

In general, cavitation is of unsteady nature (i.e. the cavity extent and volume varies with time) due to either non-uniform inflow or unsteady body motion. In this work, the cavity surface is determined in the framework of a moving mixed boundary-value problem. For a given cavitation number, the extent and

thickness of the cavity surface at a given time step is determined in an iterative manner until both the prescribed pressure and flow tangency condition are satisfied. Although the emphasis is on lifting surface, the method is in general, enough to deal with arbitrary geometries (e.g. bluff bodies, bodies of revolution, bubble dynamics).

Cavitating or free-streamline flows were first addressed in non-linear theory via the hodograph technique introduced by Helmholtz, Kirchoff and Levi-Civita (Birkhoff and Zarantonello, 1957). The cavity surface in steady flow was taken as a streamline with constant pressure (thus, constant velocity). Due to the difficulty of the hodograph technique in dealing with general body shapes, very few cases have been treated analytically. The hodograph technique was extended numerically to treat arbitrary geometries (Wu and Wang, 1964) and later applied to the analysis of supercavitating hydrofoils in the presence of a free surface (Furuya, 1975). This method, however, still could not treat general three-dimensional geometries.

The linearized cavity theory was introduced by Tulin (1953) and quickly became very popular, as evident by the vast amount of publications [1] in which it has been used. Unfortunately, linearized theory tends to grossly over-predict the thickness and extent of cavities for thick hydrofoils. It is well-known that thick hydrofoils with round leading edge tends to delay cavitation inception, consequently resulting in smaller cavities. In Kinnas (1985, 1991), a *leading edge correction* was introduced to account for the defect of linear theory at the round foil leading edge. The short cavity theory was then developed by considering the cavitating flow as a small perturbation on the non-linear fully wetted flow (Tulin and Hsu, 1980). Thus, the non-linear foil thickness effects were included in this formulation. As the thickness of a partially cavitating hydrofoil increased, the cavity size predicted by the short cavity theory reduced substantially for fixed flow conditions.

Due to the above mentioned defect of linear cavity theory, various boundary element methods (BEMs) have emerged. Pioneers in the application of BEM to propeller flow problems include Gibson and Lewis (1973) and Hess and Valarezo (1985) using velocity-based techniques, and Kerwin *et al.* (1987) and Lee (1987) using potential-based techniques. In addition to the fundamental difference between velocity- and potential-based methods, various combinations of source, vortex, and dipole singularities were also employed. A surface vorticity technique was employed by Uhlman (1987, 1989) to analyze cavitating hydrofoils. They applied the exact boundary conditions on the cavity and the foil surface, and an end-plate cavity termination model was implemented. The reduction of the cavity size as the foil thickness increased was predicted, but not as drastic as that predicted in Tulin and Hsu (1980). A surface vorticity technique to deal with thick foil sections which employed an open cavity model was developed in Yamaguchi and Kato (1983). Similar BEM techniques were developed by Lemonnier and Rowe (1988) and Rowe and

Blottiaux (1993). Potential-based BEMs were finally applied by Kinnas and Fine (1991, 1993) and Lee *et al.* (1992) for the analysis of cavitating propeller flows. It demonstrated much faster convergence characteristics than velocity-based BEMs. In particular, the solution from the first non-linear iteration where the cavity panels are placed on the foil surface beneath the cavity was found to be very close to the converged non-linear solution (Kinnas and Fine, 1990, 1993).

The potential-based BEM developed by Kinnas and Fine (1990, 1993) was later extended to predict mixed cavitation patterns on the back of propeller blades subjected to non-axisymmetric inflows (Fine and Kinnas, 1993b; Kinnas and Fine, 1992). The time-dependent cavities were assumed to detach at the blade leading edge, and a simplified wake alignment procedure (Greeley and Kerwin, 1982) was applied. The method, named PROPCAV, was later extended to predict midchord cavitation on either the back or the face of propeller blades by Mueller and Kinnas (1999).

In the present work, PROPCAV is further extended to predict cavities on either or both sides of the blade surface. The method is also capable of predicting cavitating or ventilated flow around hydrofoils and propeller blades with non-zero trailing edge thickness.

2. Formulation

The formulation for cavitating propellers is presented in Kinnas and Fine (1993) and Young and Kinnas (2001, 2003), and is summarized here for the sake of completeness. The formulation for 3D cavitating hydrofoils is very similar, details of which are presented in Kinnas and Fine (1993).

Consider a cavitating propeller subjected to a general inflow wake $\vec{q}_{\mathrm{w}}(x_s, y_s, z_s)$ [2], as shown in Figure 3. The inflow velocity, $\vec{q}_{\mathrm{in}}$, with respect to the propeller fixed coordinates (x, y, z), can be expressed as the sum of the inflow wake velocity, $\vec{q}_{\mathrm{w}}$, and the propeller's angular velocity $\vec{\omega}$, at a given location $\vec{x}$:

$$\vec{q}_{\mathrm{in}}(x, y, z, t) = \vec{q}_{\mathrm{w}}(x, r, \theta_B - \omega t) + \vec{\omega} \times \vec{x} \tag{1}$$

where $r = \sqrt{y^2 + z^2}$, $\theta_{\mathrm{B}} = \arctan(z/y)$, and $\vec{x} = (x, y, z)$. The resulting flow is assumed to be incompressible and inviscid. Hence, the total velocity, $\vec{q}$, can be expressed in terms of $\vec{q}_{\mathrm{in}}$ and the perturbation potential, ϕ:

$$\vec{q}(x, y, z, t) = \vec{q}_{\mathrm{in}}(x, y, z, t) + \nabla\phi(x, y, z, t) \tag{2}$$

where ϕ satisfies the Laplace's equation in the fluid domain (i.e. $\nabla^2\phi = 0$). Note that the propeller fixed coordinates system is used in analyzing the flow.

2.1 The boundary integral equation

The perturbation potential, ϕ, at every point p on the combined wetted blade and cavity surface, $S_{\mathrm{WB}}(t) \cup S_{\mathrm{C}}(t)$, must satisfy Green's third identity:

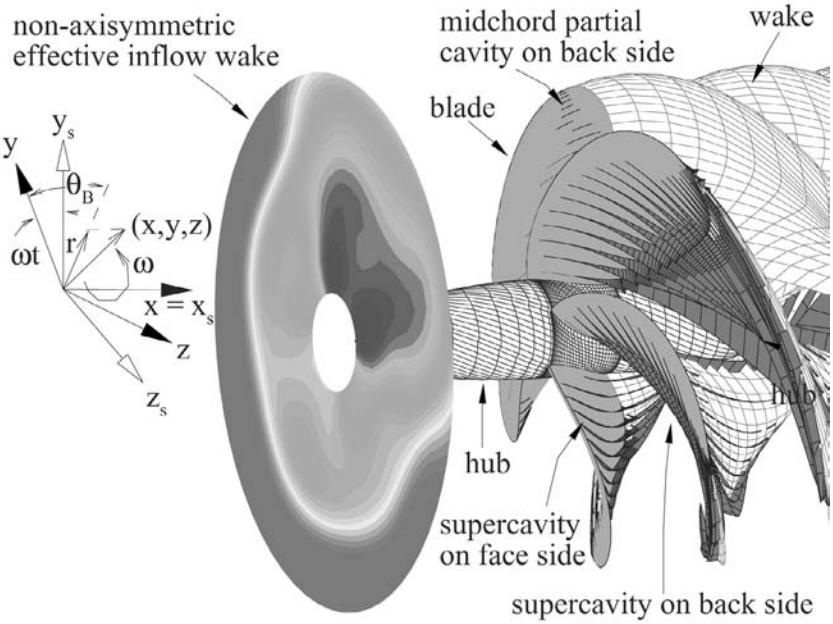

Figure 3.
Propeller subjected to a general inflow wake. The propeller fixed (x, y, z) and ship fixed (x_s, y_s, z_s) coordinate systems are shown

$$2\pi\phi_p(t) = \iint_{S_{WB}(t)\cup S_C(t)} \left[\phi_q(t)\frac{\partial G(p;q)}{\partial n_q(t)} - G(p;q)\frac{\partial \phi_q(t)}{\partial n_q(t)}\right] dS + \iint_{S_W(t)} \Delta\phi(r_q, \theta_q, t)\frac{\partial G(p;q)}{\partial n_q(t)}\, dS; \quad p \in S_{WB}(t) \cup S_C(t) \tag{3}$$

where the subscript q corresponds to the variable point in the integration. $G(p;q) = 1/R(p;q)$ is Green's function in an unbounded 3D fluid domain, with $R(p;q)$ being the distance between the points p and q. $\vec{n}_q$ is the unit vector normal to the integration surface, with the positive direction pointing into the fluid domain. $S_{WB}(t)$ denotes the wetted blade and hub surfaces, and $S_C(t)$ denotes the cavitating surfaces.

The wake surface, $S_W(t)$, is assumed to have zero thickness. The geometry of the wake surface is determined by satisfying the *force-free* wake condition, which requires zero pressure jump across the wake sheet. In this work, the wake is aligned with the circumferentially averaged inflow using a iterative lifting surface method developed by Greeley and Kerwin (1982). As stated by Greeley and Kerwin (1982), this method "artificially" suppresses the wake roll-up. Recently, a fully unsteady wake alignment method, including wake roll-up and developed tip vortex cavity, is developed for propellers in non-axisymmetric inflows (Lee and Kinnas, 2001, 2003).

The dipole strength $\Delta\phi(r, \theta, t)$ in the wake is convected along the assumed wake model with angular speed, ω:

$$\Delta\phi(r, \theta, t) = \Delta\phi_T\left(r_T, t - \tfrac{\theta-\theta_T}{\omega}\right); \quad t \geq \tfrac{\theta-\theta_T}{\omega}$$
$$\Delta\phi(r, \theta, t) = \Delta\phi^S(r_T); \quad t < \tfrac{\theta-\theta_T}{\omega} \tag{4}$$

where (r, θ) are the cylindrical coordinates at any point in the trailing wake surface (S_W), and (r_T, θ_T) are trailing edge coordinates of the corresponding streamline. $\Delta\phi^S$ is the steady flow potential jump in the wake when the propeller is subject to the circumferentially averaged flow.

The value of the dipole strength, $\Delta\phi_T(r_T, t)$, at the trailing edge of the blade at radius r_T and time t, is given by Morino's Kutta condition (Morino and Kuo, 1974):

$$\Delta\phi_T(r_T, t) = \phi_T^+(r_T, t) - \phi_T^-(r_T, t) \tag{5}$$

where $\phi_T^+(r_T, t)$ and $\phi_T^-(r_T, t)$ are the values of the potential at the upper (suction side) and lower (pressure side) blade trailing edge, respectively, at time t.

Recently, an iterative pressure Kutta condition (Kinnas and Hsin, 1992) is applied instead for the analysis of unsteady fully wetted and cavitating propellers. The iterative pressure Kutta condition modifies $\Delta\phi_T(r_T, t)$ from that of Morino to achieve equality of pressures at both sides of the trailing edge everywhere on the blade (Young *et al.*, 2001).

Note that equation (3) is a Fredholm singular integral equation of the second kind. It should be applied on the "exact" cavity surface S_C, as shown on the left of Figure 4. However, the cavity surface is not known and has to be determined as part of the solution. In this work, an approximated cavity

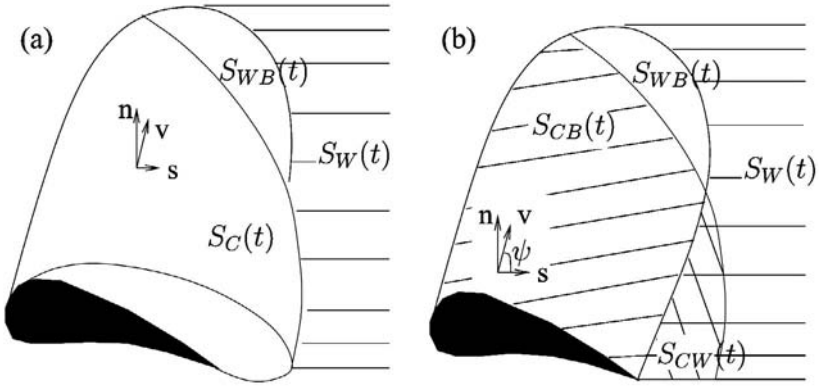

Figure 4.
Left: definition of the exact surface. Right: definition of the approximated cavity surface (Young and Kinnas, 2001)

surface, shown on the right of Figure 4, is used. The approximated cavity surface is comprised of the blade surface underneath the cavity on the blade, $S_{CB}(t)$, and the portion of the wake surface which is overlapped by the cavity, $S_{CW}(t)$. The justification for using the approximated cavity surface is based on the fast convergence characteristic of the potential-based BEM, which is demonstrated in Figure 5. In the fully non-linear scheme, cavity panels are updated at every iteration. In the present (hybrid) scheme, cavity panels are placed on the approximated cavity surface, which is equivalent to the first iteration of the fully non-linear scheme. As shown in Figure 5, the hybrid scheme predicted the cavity shape within reasonable accuracy. Additional validation studies for the hybrid scheme were presented in Fine and Kinnas (1993a).

Using the approximated cavity surface, equation (3) may be decomposed into a summation of integrals over the blade surface, $S_B \equiv S_{CB}(t) + S_{WB}(t)$, and the portion of the wake surface which is overlapped by the cavity, $S_{CW}(t)$, as shown in Figure 4:

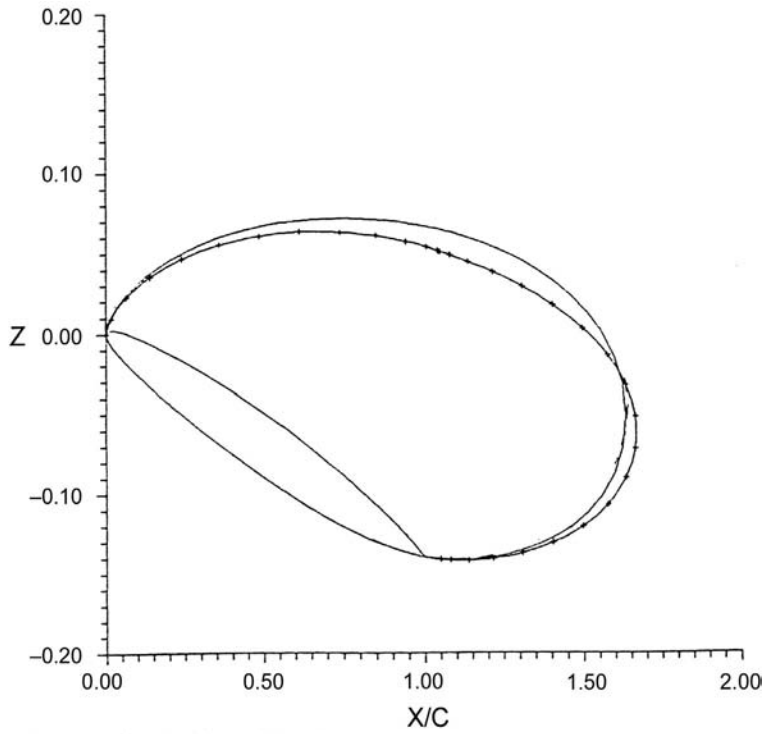

Source: Fine & Kinnas (1993a)

Figure 5.
Comparison of predicted cavity shapes from the fully non-linear (solid) and the present hybrid (solid with dots) scheme for NACA16004 at $\alpha = 6°$. $\alpha/\sigma = 0.44$

$$\left\{\begin{array}{l} p \in S_{\mathrm{B}}\colon\ \ 2\pi\phi_{\mathrm{p}}(t) = 0 \\ p \in S_{\mathrm{CW}}(t)\colon\ \ 4\pi\phi_{\mathrm{p}}^{\pm}(t) = \pm 2\pi\Delta\phi_{\mathrm{p}}(t) \end{array}\right\} + \iint_{S_{\mathrm{B}}}\left[\phi_q(t)\frac{\partial G(p;q)}{\partial n_q} - G(p;q)\frac{\partial \phi_q(t)}{\partial n_q}\right]\mathrm{d}S - \iint_{S_{\mathrm{CW}}(t)}\left[\frac{\partial \phi^{+}}{\partial n}(t) - \frac{\partial \phi^{-}}{\partial n}(t)\right]G(p;q)\,\mathrm{d}S + \iint_{S_{\mathrm{CW}}(t)\cup S_{\mathrm{W}}(t)}\Delta\phi(r_q,\theta_q,t)\frac{\partial G(p;q)}{\partial n_q}\,\mathrm{d}S \tag{6}$$

where the superscripts "+" and "−" denote the upper and lower wake surface, respectively.

2.2 Boundary conditions

Equation (6) implies that the perturbation potential (ϕ_{p}) can be expressed as: continuous source (G) and dipole ($\partial G/\partial n$) distributions on the wetted blade (S_{WB}) and cavity ($S_{\mathrm{CB}} \cup S_{\mathrm{CW}}$) surfaces, and continuous dipole distribution on the wake surface, S_{W}. Thus, ϕ_{p} can be uniquely determined by satisfying the following boundary conditions.

2.2.1 Kinematic boundary condition on wetted blade and hub surfaces. The kinematic boundary condition requires the flow to be tangent to the wetted blade and hub surface, which forms a Neumann-type boundary condition for $\partial\phi/\partial n$:

$$\frac{\partial \phi}{\partial n} = -\vec{q}_{\mathrm{in}} \cdot \vec{n}. \tag{7}$$

2.2.2 Dynamic boundary condition on cavitating surfaces. The dynamic boundary condition on the cavitating blade and wake surfaces requires the pressure everywhere on the cavity to be constant and equal to the vapor pressure, P_{v}. By applying Bernoulli's equation, the total cavity velocity, $\vec{q}_{\mathrm{c}}$, can be expressed as follows:

$$|\vec{q}_{\mathrm{c}}|^2 = n^2D^2\sigma_n + |\vec{q}_{\mathrm{w}}|^2 + \omega^2 r^2 - 2gy_{\mathrm{s}} - 2\frac{\partial \phi}{\partial t} \tag{8}$$

where $\sigma_n \equiv (P_o - P_v)/((\rho/2)n^2D^2)$ is the cavitation number; ρ is the fluid density and r is the distance from the axis of rotation. P_o is the pressure far upstream on the shaft axis; g is the acceleration of gravity and y_{s} is the ship fixed coordinate, shown in Figure 3. $n = \omega/2\pi$ and D are the propeller rotational frequency and diameter, respectively.

The total cavity velocity can also be expressed in terms of the local derivatives along the s (chordwise), v (spanwise), and n (normal) grid directions:

$$\vec{q}_c = \frac{V_s[\vec{s} - (\vec{s}\cdot\vec{v})\vec{v}] + V_v[\vec{v} - (\vec{s}\cdot\vec{v})\vec{s}]}{\|\vec{s} \times \vec{v}\|^2} + (V_n)\vec{n} \tag{9}$$

where $\vec{s}$, $\vec{v}$, and $\vec{n}$ denote the unit vectors along the non-orthogonal curvilinear coordinates s, v, and n, respectively. The total velocities on the local coordinates (V_s, V_v, V_n) are defined as follows:

$$V_s \equiv \frac{\partial \phi}{\partial s} + \vec{q}_{\text{in}}\cdot\vec{s}; \quad V_v \equiv \frac{\partial \phi}{\partial v} + \vec{q}_{\text{in}}\cdot\vec{v}; \quad V_n \equiv \frac{\partial \phi}{\partial n} + \vec{q}_{\text{in}}\cdot\vec{n} \tag{10}$$

Note that if s, v, and n were located on the "exact" cavity surface, then the total normal velocity, V_n, would be zero. However, this is not the case since the cavity surface is approximated with the blade surface beneath the cavity and the wake surface overlapped by the cavity. Although V_n may not be exactly zero on the approximated cavity surface, it is small enough to be neglected in the dynamic boundary condition (Fine, 1992).

Equations (8) and (9) can be integrated to form a quadratic equation in terms of the unknown chordwise perturbation velocity $\partial\phi/\partial s$. By selecting the root which corresponds to the cavity velocity vectors that point downstream, the following expression can be derived:

$$\frac{\partial \phi}{\partial s} = -\vec{q}_{\text{in}}\cdot\vec{s} + V_v \cos\psi + \sin\psi\sqrt{|\vec{q}_c|^2 - V_v^2} \tag{11}$$

where ψ is the angle between s and v directions, as shown in Figure 4. Equation (11) can then be integrated to form a Dirichlet type boundary condition for ϕ.

It should be noted that the terms $\partial\phi/\partial t$ and $\partial\phi/\partial v$ inside $|\vec{q}_c|$ and V_v in equation (11) are also unknown and are determined in an iterative manner (Fine, 1992; Kinnas and Fine, 1993). Initially, the total flow velocity is assumed to be tangent to the s coordinate, i.e. $\partial\phi/\partial v = |\vec{q}_c|(\vec{s}\cdot\vec{v}) - \vec{q}_{\text{in}}\cdot\vec{v}$. In subsequent iterations, $\partial\phi/\partial v$ is calculated via a second order central difference scheme of the potential in the $\vec{v}$ direction. Iterations are carried out until the change in $\partial\phi/\partial v$ is less than a prescribed tolerance. $\partial\phi/\partial t$ is assumed to be zero in the first two propeller revolutions. In subsequent revolutions, $\partial\phi/\partial t$ is calculated via a second order moving least square method (Tabbara *et al.*, 1994) using the previous ϕ when the key blade was in the same angular position.

On the cavitating wake surface, the coordinate s is assumed to follow the streamlines. It was found that the crossflow term ($\partial/\partial v$) in the cavitating wake region had a very small effect on the solution (Fine, 1992; Fine and Kinnas, 1993b). Thus, the total cross flow velocity is assumed to be small, which renders the following expression on the cavitating wake surface:

$$\frac{\partial \phi}{\partial s} = -\vec{q}_{\text{in}} \cdot \vec{s} + |\vec{q}_{\text{c}}|. \tag{12}$$

2.2.3 Kinematic boundary condition on cavitating surfaces. The kinematic boundary condition requires that the total velocity normal to the cavity surface to be zero:

$$\frac{D}{Dt}(n - h(s, v, t)) = \left[\frac{\partial}{\partial t} + \vec{q}_{\text{c}}(x, y, z, t) \cdot \nabla\right](n - h(s, v, t)) = 0 \tag{13}$$

where n and h are the curvilinear coordinate and cavity thickness normal to the blade surface, respectively.

Substituting equation (9) into equation (13) yields the following partial differential equation for h on the blade (Kinnas and Fine, 1993):

$$\frac{\partial h}{\partial s}\left[V_s - \cos\psi V_v\right] + \frac{\partial h}{\partial v}\left[V_v - \cos\psi V_s\right] = \sin^2\psi\left(V_n - \frac{\partial h}{\partial t}\right) \tag{14}$$

Assuming again that the spanwise crossflow velocity on the wake surface is small, the kinematic boundary condition reduces to the following equation for the cavity thickness (h_{w}) in the wake:

$$\left[\frac{\partial \phi^+}{\partial n} - \frac{\partial \phi^-}{\partial n}\right] - \frac{\partial h_{\text{w}}}{\partial t} = |\vec{q}_{\text{c}}|\frac{\partial h_{\text{w}}}{\partial s} \tag{15}$$

Note that h_{w} in equation (15) is defined normal to the wake surface. In addition, the quantity h_{w} at the blade trailing edge is determined by interpolating the upper and/or lower cavity surface over the blade and computing its normal offset from the wake sheet.

2.2.4 Cavity closure condition. The extent of the unsteady cavity is unknown and has to be determined as part of the solution. The cavity length at each radius r and time t is given by the function $l(r, t)$. For a given cavitation number, σ_n, the cavity planform, $l(r, t)$, must satisfy the following condition:

$$\delta(l(r, t); r, \sigma_n) = 0 \tag{16}$$

where δ is the thickness of the cavity trailing edge. Equation (16) requires that the cavity closes at its trailing edge. This requirement is the basis of a Newton-Raphson iterative method that is used to find the cavity planform (Kinnas and Fine, 1993).

2.2.5 Cavity detachment condition. The cavity detachment locations are determined iteratively by satisfying the Villat-Brillouin smooth detachment condition (Brillouin, 1911; Villat, 1914). This condition requires that the cavities do not intersect the blade at its leading edge, and the pressure upstream of the cavities to be greater than the vapor pressure. It should be noted that the

current formulation assumes the flow to be inviscid. It is widely known that viscosity affects the cavity detachment, as well as the extent and thickness of the cavity. However, investigations by Kinnas *et al.* (1994) concluded that the effect of viscosity on the predicted cavity extent and volume is negligible for the case of supercavitation, as shown in Figure 6.

2.3 Numerical aspects

The unsteady cavity problem is solved by inverting equation (6) subject to equations (4), (5), (7), (11), (12) and (16), and the cavity detachment condition. The integral surfaces are approximated with hyperboloidal panels (Kinnas and Hsin, 1992) on which constant strength dipoles and sources are distributed. The present low-order BEM approach is an extension of those of Kerwin *et al.* (1987)

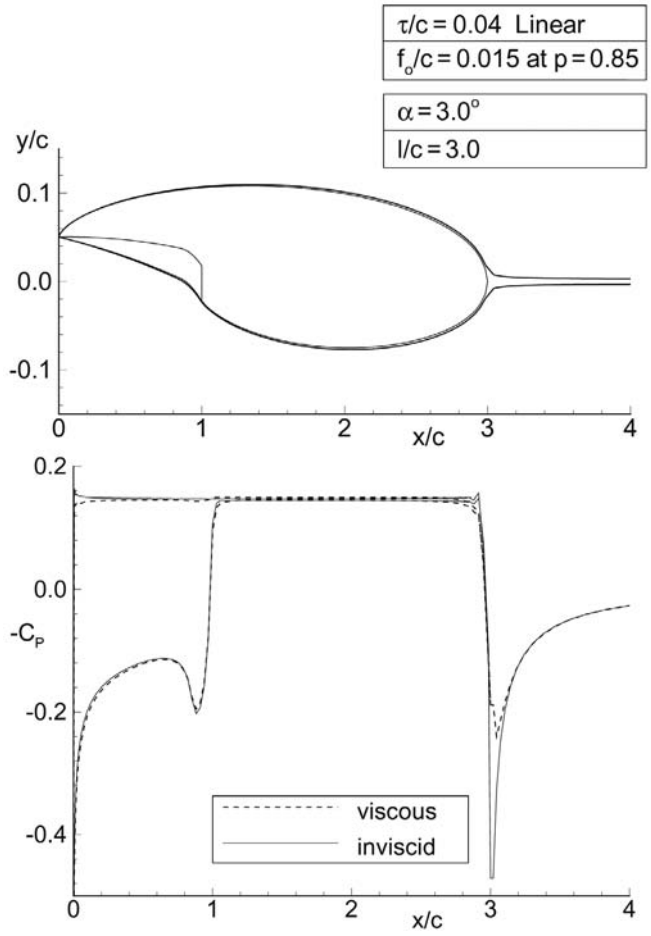

Source: Kinnas *et al.* (1994)

Figure 6.
Supercavitating hydrofoil in inviscid and viscous flow at $Re = 2 \times 10^7$. Cavity shape and boundary layer displacement thickness (top); pressure distributions (bottom)

and Kinnas and Hsin (1992), in the cases of steady and unsteady non-cavitating (also called wetted) flows around propeller blades, respectively. The low-order method has been applied in the cases of blades with thin sections and/or extreme skew, and the results have been found to converge quickly with number of panels (Hsin, 1990, Hsin *et al.*, 1991, Kerwin *et al.*, 1987; Kinnas and Hsin, 1992, 1994, Kinnas *et al.*, 1993, Lee, 1987). Equation (6) is applied at the panel centroids in order to determine the potentials at each panel. The problem is solved in the time domain with constant time step size Δt.

The numerical implementation is described in detail in Kinnas and Fine (1993). In brief, for a given cavity planform, Green's formula is solved with respect to unknown ϕ on the wetted blade and hub surfaces, and unknown $\partial\phi/\partial n$ on the cavitating surfaces. The cavity heights on the blade and the wake are computed by numerically differentiating equations (14) and (15) with a second order central finite difference method. At each time step, Newton-Raphson iterations are performed to determine the cavity lengths which satisfy the cavity closure condition equation (16) for the given guess of cavity detachment locations. An example of the iteration procedure performed within each time step on a cavitating foil section is shown on the left part of Figure 7. At the end of every time step, the cavity detachment locations are adjusted via the smooth detachment condition, as explained in the earlier section. An example of the convergence of cavity shape with number of time steps on a foil section is also shown in Figure 7. It should be noted that in the case of steady inflow, only one time step is performed per propeller revolution, and that the cavity detachment locations are adjusted in every time step. The converged cavity planform and cavitating pressure distributions for a 3D hydrofoil is shown on the right part of Figure 7. Note that the current method is able to search for cavities on both sides of the foil surface. In addition, note the influence of cavity detachment locations on the predicted cavity shape and pressure distribution.

In order to save the computational time, the solution at each time step is only obtained for the *key* blade in the case of a cavitating propeller. The influence of each of the other blades is accounted for in a progressive manner by using the solution from an earlier time step when the key blade was in the position of that blade.

A very crucial issue in the numerical implementation was found to be the treatment of panels which were intersected by the cavity trailing edge. In order to avoid recomputing influence coefficients, a *split* panel technique (Fine, 1992; Kinnas and Fine, 1993) was devised. The intersected panel is treated as one panel with ϕ and $\partial\phi/\partial n$ determined as weighted averages of the values on the wetted and the cavitating part of the panel. This technique, as depicted in Figure 8, provided substantial savings on computing time since the same panel discretization can handle arbitrary cavity planforms.

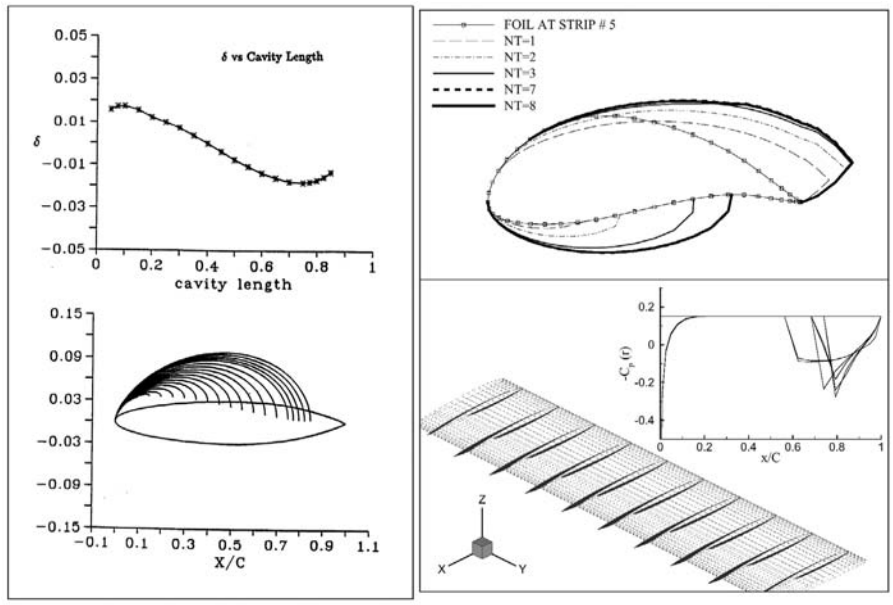

Note: Left: Convergence of predicted cavity shape and cavity trailing edge openness, δ, with number or iterations within a time step where the cavity for that strip is assumed to detach from the foil leading edge. From (Kinnas & Fine 1993). Right: Convergence of the predicted cavity shape with number of time steps (NT) for the middle strip, and the converged cavity planform and cavitating pressure distributions for a 3-D hydrofoil. Notice that the current method is able to search for cavities on both sides of the foil surface. In addition, notice the influence of cavity detachment locations on the predicted cavity shape and pressure distribution

Figure 7.

3. Supercavitating propellers and hydrofoils

The speed limit for classical fully submerged propellers is approximately 20-25 knots. They do not perform well at higher speeds because considerable amount of cavitation is unavoidable. Supercavitating propellers, on the other hand, operate in fully cavitating conditions. The term supercavity refers to a cavity that is longer than the chord length of the blade. Supercavitating propellers tend to have very sharp leading edges and very blunt trailing edges. They are more efficient than classical non-cavitating or partially cavitating propellers because of:

- reduction in viscous drag due to the un-wetted suction side as a result of the supercavity, and
- reduction in noise and blade surface erosion as a result of smaller volume change and cavities that collapse downstream of the blade trailing edge.

However, supercavitating blade sections are difficult to model due to the unknown physics following the blunt trailing edge. Experimental evidence shows that the separated zone behind the thick blade trailing edge forms a closed cavity that separates from the practically ideal irrotational flow around

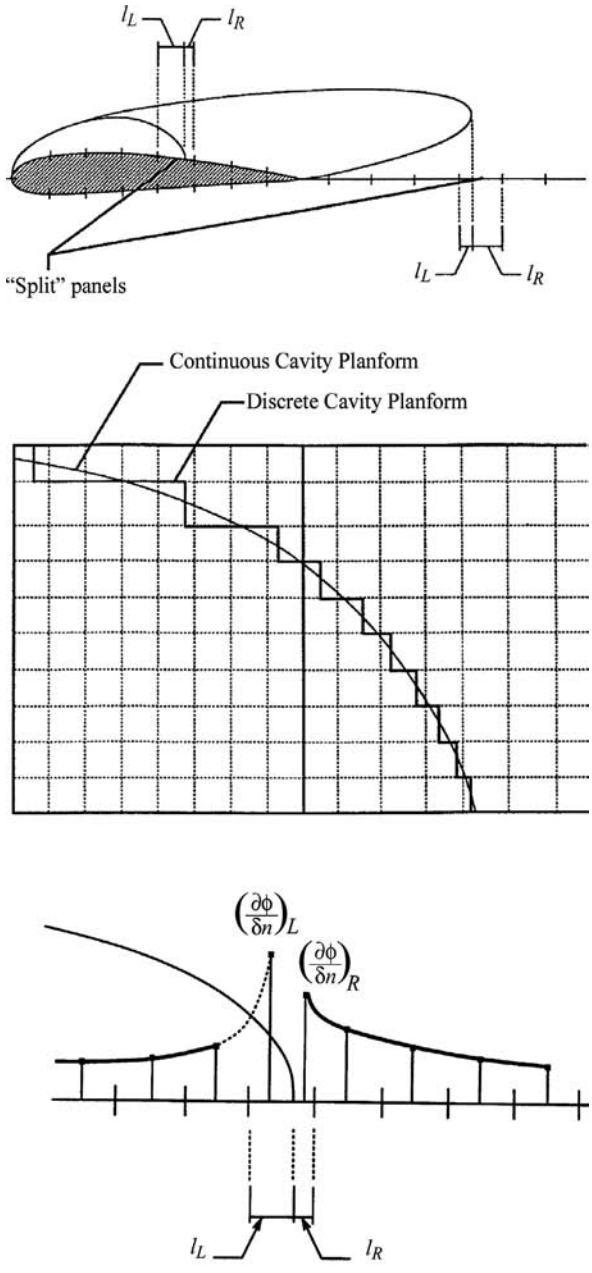

Note: Fine & Kinnas (1993a)

Figure 8.
The split panel technique

a supercavitating blade section (Russel, 1958). Furthermore, the pressure within the separated zone (also called the base pressure) can be assumed to be uniform (Riabouchinsky, 1926; Tulin, 1953). However, the extent of the separated zone and the base pressure are unknown.

In this work, the base pressure is assumed to be constant and equal to the vapor pressure. Thus, the extent and thickness of the separated region can be solved like an additional cavitation bubble. This assumption is valid in the case of supercavitation. In the case when part of the blade is fully wetted or partially cavitating, this assumption should still be a reasonable approximation since the pressure change along the blade trailing edge should be smooth. To avoid "openness" at the blade trailing edge, a small initial closing zone, shown in Figure 9, is introduced. The precise geometry of the initial closing zone is not important, as long as it is inside the separated region and its trailing edge lies on the aligned wake sheet. The method is modified so that it treats the original blade and the initial closing zone as one solid body, both of which do not change with time. The size and the extent of the cavities and the separated region are allowed to change with time, and are determined as part of the solution. The treatment of non-zero trailing edge sections in fully wetted, partially cavitating, and supercavitating conditions are depicted in Figure 9. Cavitation patterns that can be predicted by the present method are shown in Figure 10. Details of the formulation and validation studies are given in Young and Kinnas (2002a, 2003). It should be noted that the current method can also

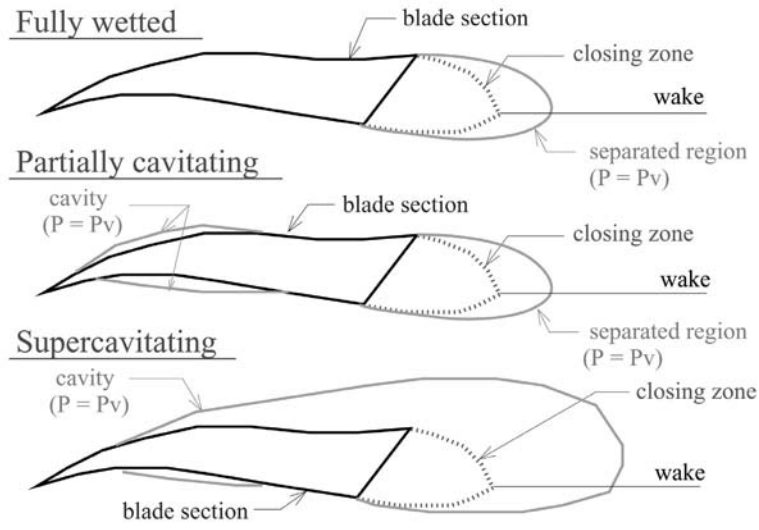

Source: Young & Kinnas (2003)

Figure 9.
Treatment of non-zero trailing edge sections in fully wetted, partially cavitating, and supercavitating conditions

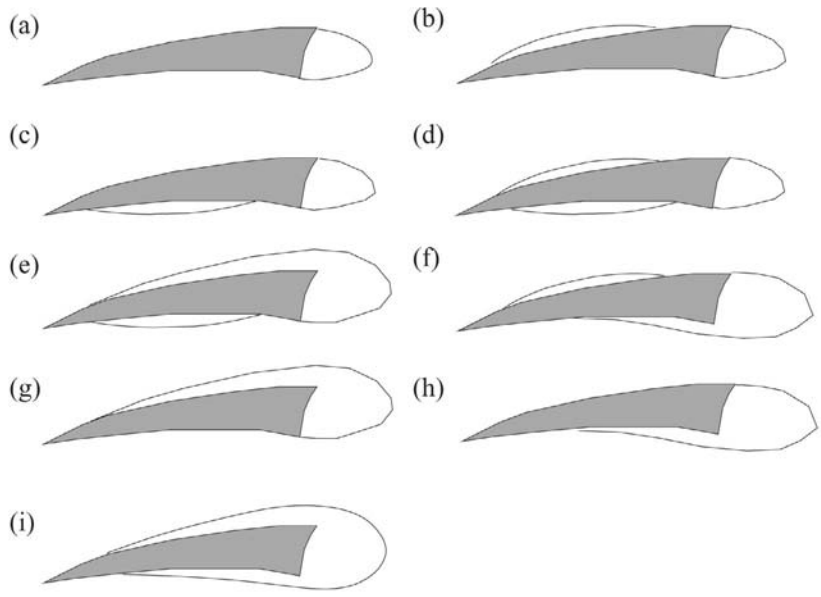

Source: Young & Kinnas (2003)

Figure 10.
Cavitation patterns that can be predicted by the present method

be applied to ventilated hydrofoils by replacing the vapor pressure with the ventilation pressure.

4. Numerical validation

4.1 Convergence with number of panels

In order to validate the method, extensive parametric studies were performed for various propeller (Young and Kinnas, 2001, 2002b, 2003) and hydrofoil geometries (Kinnas and Fine, 1993, Young and Kinnas, 2002a) in steady and unsteady flow conditions. For the sake of completeness, convergence studies of the method using a 3D hydrofoil is shown in this section. The delta shape hydrofoil, shown in Figure 11, has a constant chord to span ratio of 1:4. The maximum sweep to span ratio is 0.2. The foil has a linear thickness distribution with a maximum thickness to chord ratio of 0.0698, and a parabolic camber distribution with a maximum camber to chord ratio of 0.03. The flow conditions are as follows: $\sigma_v = (P_o - P_v)/\left(\rho/2V_A^2\right) = 0.3$ and $\alpha = 4°$. For the analysis of hydrofoils, the symbols V_A and α denote the inflow velocity and the angle of attack, respectively. Comparisons of the predicted cavity planforms for three different grid discretization are shown in Figure 11.

4.2 Multiplicity of solutions

It is well-known that some cavitation numbers produce multiple solutions, which can be confirmed from observed instabilities on cavity extents during

2D and 3D experiments. The current method is able to predict multiple solutions in 3D (Kinnas and Fine, 1992, 1993), as shown in Figure 12. The hydrofoil is the same as described Section 4.1, but it has a rectangular planform and $\alpha = 3°$. Note that at $\sigma_v = 0.385$, two cavity planforms are predicted, one partial cavity and one mixed cavity (slightly supercavity at midspan). The partial cavity is produced by applying an initial guess of cavity length which equals to 20 percent of the chord length, and the mixed cavity is produced by applying an initial guess of cavity length which equals to 120 percent of the chord length. The cavity length (non-dimensionalized by the chord length) at midchord versus α/σ_v is shown in Figure 13. It is worth noting that Figure 13 carries striking similarity to the well-known characteristic curve for a 2D cavitating flat plate, which is not presented in this paper.

4.3 Sample run with face and back cavitation

In order to show the method's ability to search for simultaneous face and back cavitation, results from a sample run using the same hydrofoil is shown in this section. The flow conditions for the hydrofoil are as follows: $\sigma_v = 0.085$ and $\alpha = 0.3°$. As shown in Figure 14, there is midchord supercavity on the suction side and leading edge partial cavitation on the pressure side. The corresponding pressure distributions along the spanwise direction are shown in Figure 15. Note that the partial cavity on the face side significantly alters the pressure distribution, which in turn alters the force acting on the hydrofoil. Thus, it is crucial to search for cavities on both sides of the blade surface, and to determine the correct cavity detachment locations.

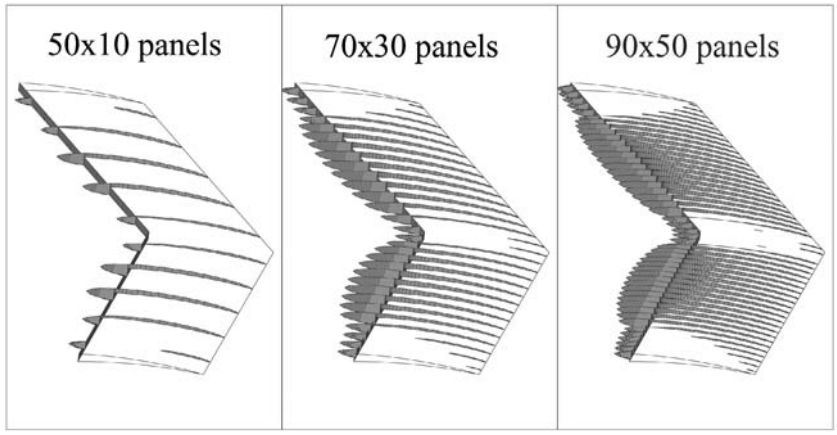

Figure 11.
Convergence of predicted cavity planform with number of panels. Maximum sweep to span ratio = 0.2, σ_v=0.3 and $\alpha = 4°$

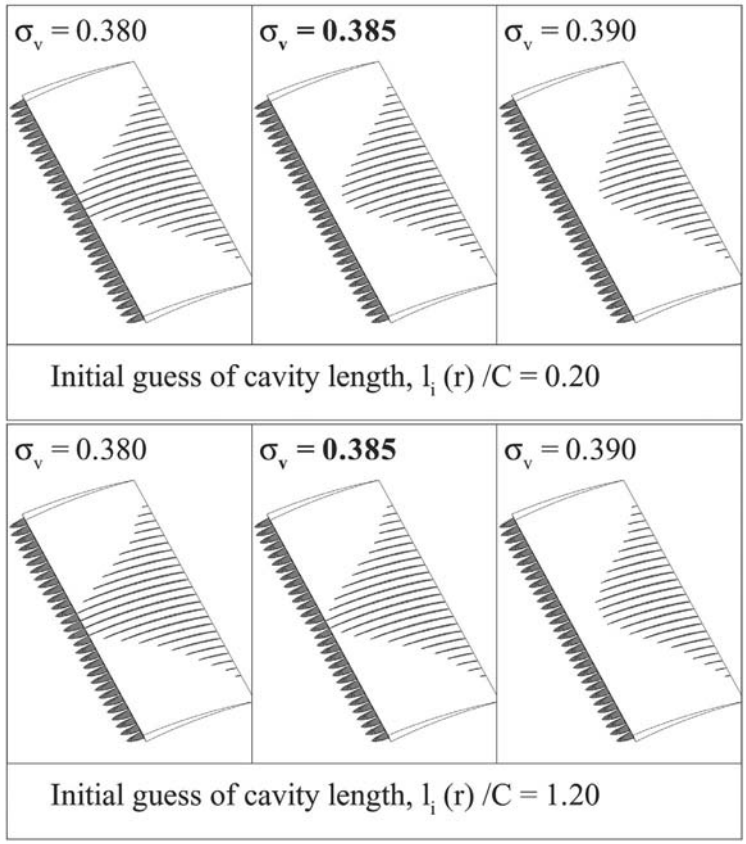

Note: The shaded regions following the blade trailing edge are the separated zones

Figure 12.
Multiple solutions in 3D for $\sigma_v = 0.385$, $\alpha = 3°$ and 70×30 panels

5. Experimental validations

5.1 Highly skewed propeller

In order to validate the panel method, numerical predictions are compared with experimental measurements for propeller 4383, which is a five-bladed fully submerged propeller with a high skew angle of 72°. The propeller geometry is given in Boswell (1971) and Cumming *et al.* (1972), and is shown in Figure 16. Open water (non-cavitating) performance was measured at the NSRDC deep water basin, and are compared with numerical predictions by the current method in Figure 16. It should be noted that in the numerical analysis, a friction coefficient that corresponds to the blade Reynolds number was applied on the wetted portion of the blade.

Cavitation tests for propeller 4383 were conducted in a 24 in. cavitation tunnel at NSRDC (Boswell, 1971). Comparisons of predicted and measured

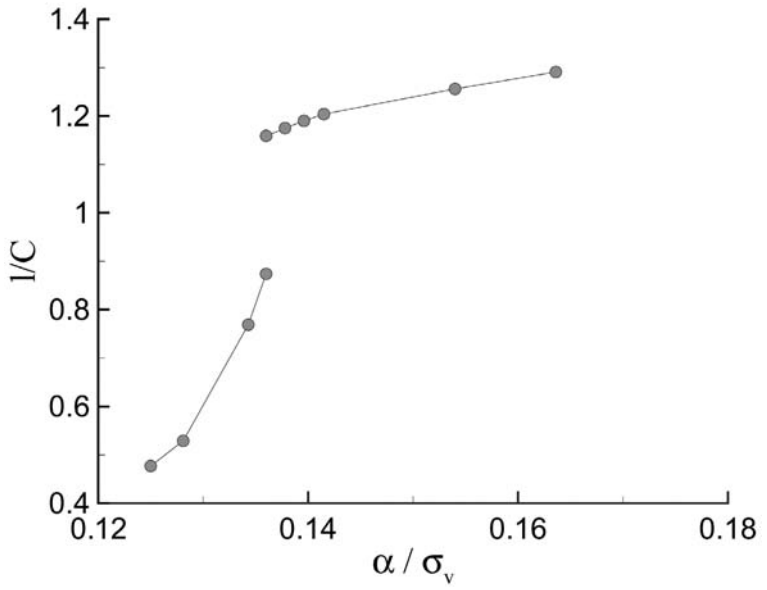

Figure 13.
Cavity length at midspan vs α/σ_v for a 3D hydrofoil. α=3°. 70 × 30 panels

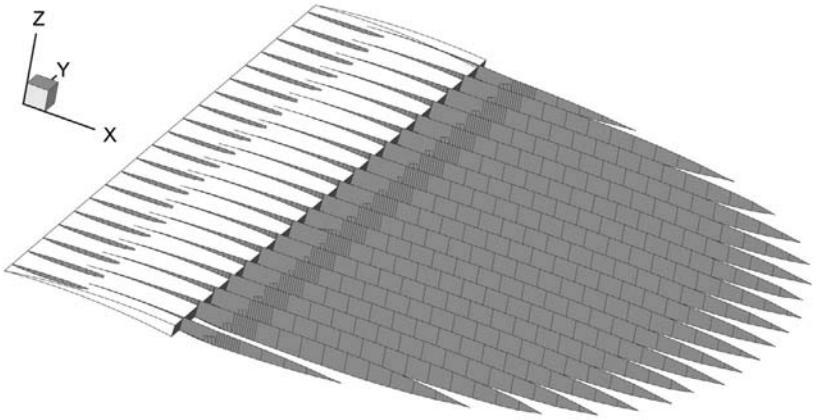

Figure 14.
Outline of 3D hydrofoil and predicted cavity planform. σ_v=0.085. α = 0.3°. 60 × 20 panels

thrust ($K_T = T/\rho n^2 D^4$) and torque ($K_Q = Q/\rho n^2 D^5$) coefficients as a function of advance ratio ($J_A = V_A/nD$) and cavitation number ($\sigma_v = (P_o - P_v)/(0.5\rho V_A^2)$) are shown in Figure 17. For the analysis of propeller flows, the symbol V_A denotes the advance speed of the propeller in open water. Examples of the predicted cavity planforms for $\sigma_v = 3.0$ and $J_A = 0.5$-0.7 are shown in Figure 18. As shown in Figures 16 and 17, the numerical predictions compared well with experimental measurements. It should be noted that the comparison for $\sigma_v = 1.0$ shown in Figure 17 has been improved considerably

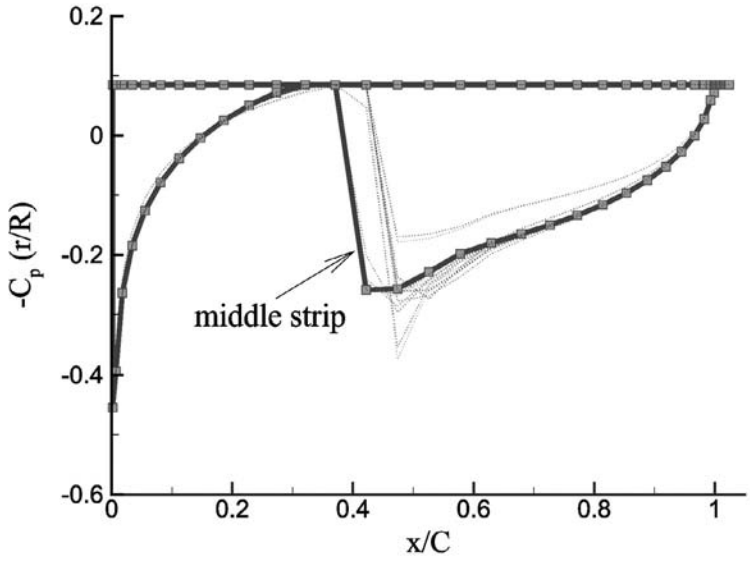

Note: Notice the partial cavity on the face side significantly alters the pressure distribution, which in turn alters the force acting on the hydrofoil

Figure 15.
Predicted cavitating pressure distributions along the spanwise direction. $\sigma_v = 0.085$. $\alpha = 0.3°$. 60×20 panels

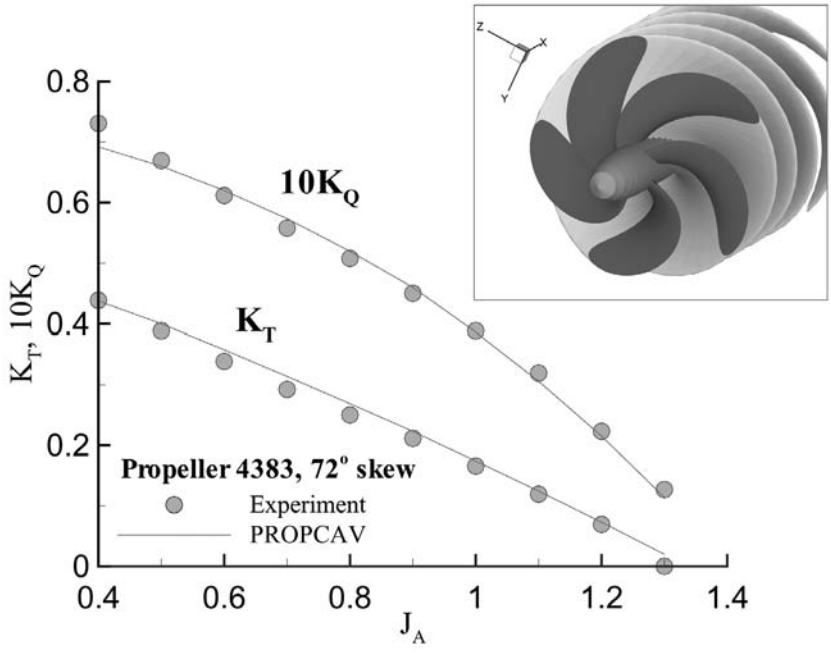

Figure 16.
Predicted and measured open water (non-cavitating) performance of a highly skewed propeller 4383. Also shown is the discretized propeller geometry

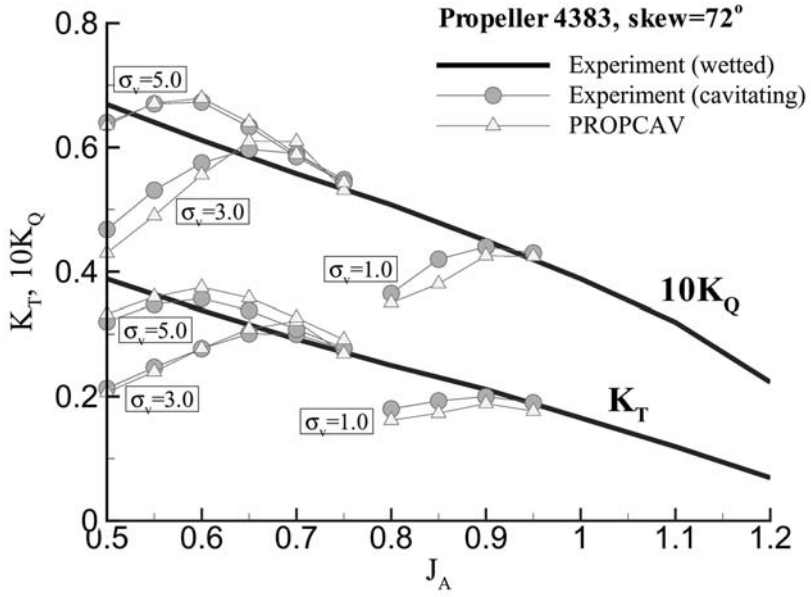

Figure 17.
Predicted and measured thrust (K_T) and torque (K_Q) coefficients as a function of cavitation number (σ_v) and advance ratio (J_A). Propeller 4383
Source: from the discussion section of Kinnas *et al.* (2002)

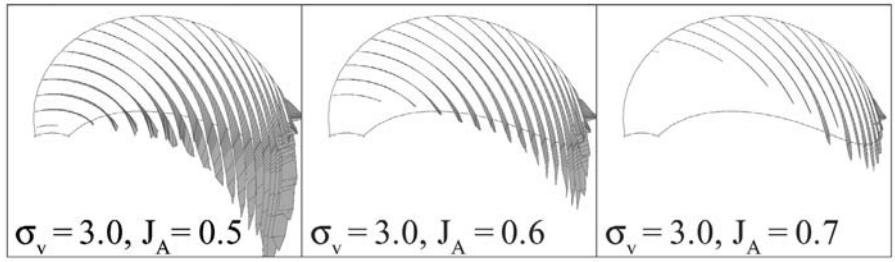

Figure 18.
Predicted cavity planforms for σ_v=3.0 and J_A=0.5-0.7. Propeller 4383

by incorporating a semi-empirical adjustment which alters the cavity detachment algorithm to account for viscous and surface tension effects. A description of this semi-empirical adjustment is given in the discussion section of Kinnas *et al.* (2002).

5.2 Supercavitating propeller

To validate the treatment of supercavitating propellers, the predicted force coefficients are compared with experimental measurements (Matsuda *et al.*, 1994) for a supercavitating propeller. The test geometry is M.P.No.345 (SRI), which is designed using SSPA charts under the following conditions: $J_A = 1.10$, $\sigma_v = 0.40$, and $K_T = 0.160$. The discretized propeller geometry is shown in Figure 19. Comparisons of the predicted and measured thrust, torque, and

efficiency ($\eta_o = K_T/K_Q J_A/2\pi$) are shown in Figure 20. As evident in the figure, the numerical predictions agree well with the experimental measurements. It should be noted that extensive parametric studies of the method were performed for this propeller, and are presented in Young and Kinnas (2003).

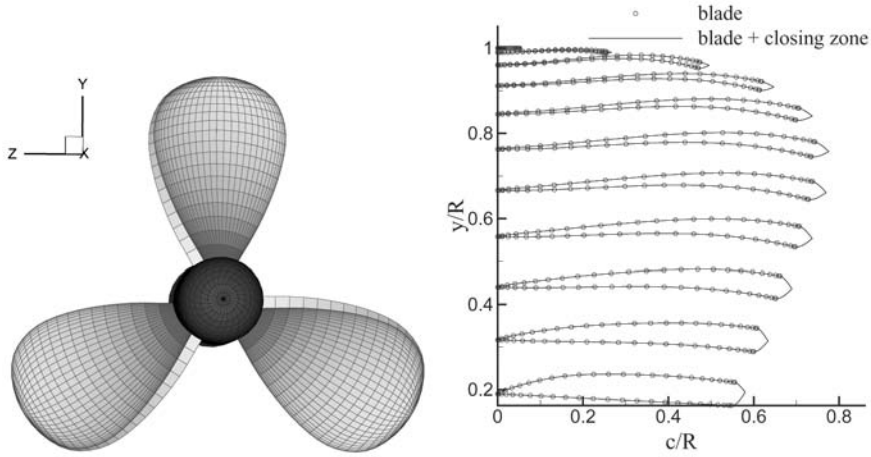

Source: Young & Kinnas (2003)

Figure 19.
Left: discretized propeller geometry. Right: blade section and initial closing zone geometry. Propeller SRI. Uniform inflow

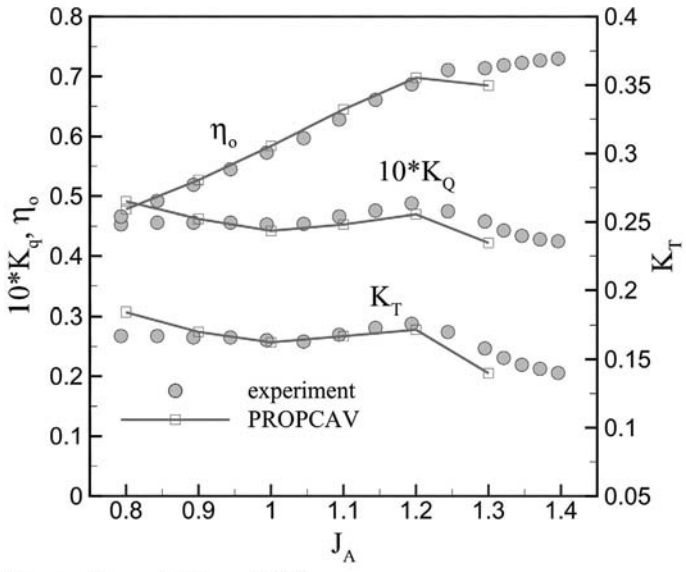

Source: Young & Kinnas (2003)

Figure 20.
Comparison of the predicted versus measured K_T, K_Q, and η_o for different advance coefficients. Propeller SRI. Uniform inflow

6. Conclusions

BEM-based techniques for the prediction of cavitating or ventilated flows around hydrofoils and propellers were described. A recent potential-based BEM that is capable of predicting simultaneous (or alternating) face and back cavitation on classical, supercavitating, and ventilated blade section geometries was presented. Extensive parametric studies and experimental validations have been performed for various propeller and hydrofoil geometries, some of which were presented in Young and Kinnas (2001, 2002b, 2003).

Current efforts include:

(1) modeling of cavitation on multi-component propulsor systems (Kinnas *et al.*, 2001, 2002);

(2) modeling of surface-piercing propellers (Young, 2002; Young and Kinnas, 2001); and

(3) modeling of developed tip vortex cavity (Lee, 2002; Lee and Kinnas, 2001).

Notes

1. An extended list of which may be found in Kinnas (1991) and Tulin and Hsu (1980).
2. $\vec{q}_w$ is assumed to be the *effective wake*, i.e. it includes the interaction between the vorticity in the inflow and the propeller (Choi, 2000; Kinnas *et al.*, 2000).

References

Birkhoff, G. and Zarantonello, E. (1957), *Jets, Wakes and Cavities*, Academic Press, New York.

Boswell, R. (1971), "Design, cavitation performance and open-water performance of a series of research skewed propellers", *Technical Report 3339*, DTNSRDC.

Brillouin, M. (1911), "Les surfaces de glissement de Helmholtz et la resistance des fluides", *Annales de Chimie and de Physique*, Vol. 23, pp. 145-230.

Choi, J. (2000), "Vortical inflow – propeller interaction using unsteady three-dimensional euler solver", Doctoral dissertation, Department of Civil Engineering, The University of Texas, Austin.

Cumming, R.A., Morgan, W.B. and Boswell, R.J. (1972), "Highly skewed propellers", *Transactions*, Society of Naval Architects and Marine Engineers.

Fine, N.E. (1992) "Nonlinear analysis of cavitating propellers in nonuniform flow", Doctoral dissertation, Department of Ocean Engineering, MIT.

Fine, N. and Kinnas, S. (1993a), "A boundary element method for the analysis of the flow around 3d cavitating hydrofoils", *Journal of Ship Research*, Vol. 37, pp. 213-24.

Fine, N. and Kinnas, S. (1993b), "The nonlinear numerical prediction of unsteady sheet cavitation for propellers of extreme geometry", *Proceedings: Sixth International Conference on Numerical Ship Hydrodynamics*, pp. 531-44.

Furuya, O. (1975), "Nonlinear calculation of arbitrarily shaped supercavitating hydrofoils near a free surface", *Journal of Fluid Mechanics*, Vol. 68, pp. 21-40.

Gibson, I. and Lewis, R.I. (1973), "Ducted propeller analysis by surface vorticity and actuator disc theory", *Proceedings of the Symposium on Ducted Propellers*, The Royal Institution of Naval Architects, Teddington, England.

Greeley, D. and Kerwin, J. (1982), "Numerical methods for propeller design and analysis in steady flow", *Trans. SNAME*, Vol. 90.

Hess, J.L. and Valarezo, W. (1985), "Calculation of steady flow about propellers by means of a surface panel method", *Proceedings: 23rd Aerospace Sciences Meeting*, AIAA, Reno, Nevada.

Hsin, C-Y. (1990), "Development and analysis of panel method for propellers in unsteady flow", Doctoral dissertation, Department of Ocean Engineering, MIT.

Hsin, C-Y., Kerwin, J. and Kinnas, S. (1991), "A panel method for the analysis of the flow around highly skewed propellers", *Proceedings: Propellers/Shafting '91 Symposium*, (paper No. 11), Soc. Naval Arch. and Marine Engnrs, Virginia Beach, VA, pp. 1-13.

Kerwin, J., Kinnas, S., Lee, J-T. and Shih, W-Z. (1987), "A surface panel method for the hydrodynamic analysis of ducted propellers", *Trans. SNAME*, Vol. 95.

Kinnas, S. (1985), "Non-linear corrections to the linear theory for the prediction of the cavitating flow around hydrofoils", Doctoral dissertation, Department of Ocean Engineering, MIT.

Kinnas, S. (1991), "Leading-edge corrections to the linear theory of partially cavitating hydrofoils", *Journal of Ship Research*, Vol. 35 No. 1, pp. 15-27.

Kinnas, S. and Fine, N. (1990), "Non-linear analysis of the flow around partially or super-cavitating hydrofoils by a potential based panel method", *Proceedings of the IABEM-90 Symposium of the International Association for Boundary Element Methods*, pp. 289-300.

Kinnas, S. and Fine, N. (1991), "Non-linear analysis of the flow around partially or super-cavitating hydrofoils by a potential based panel method", *Proceedings: Boundary Integral Methods – Theory and Applications, Proceedings of the IABEM-90 Symposium*, 15-19 October 1990, Springer-Verlag, Heidelberg, Rome, Italy, pp. 289-300.

Kinnas, S. and Fine, N. (1992), "A nonlinear boundary element method for the analysis of unsteady propeller sheet cavitation", *Proceedings: Nineteenth Symposium on Naval Hydrodynamics*, pp. 717-37.

Kinnas, S. and Fine, N. (1993), "A numerical nonlinear analysis of the flow around two- and three-dimensional partially cavitating hydrofoils", *Journal of Fluid Mechanics*, Vol. 254, pp. 151-81.

Kinnas, S. and Hsin, C-Y. (1992), "A boundary element method for the analysis of the unsteady flow around extreme propeller geometries", *AIAA Journal*, Vol. 30 No. 3, pp. 688-96.

Kinnas, S. and Hsin, C-Y. (1994), "On the local error of a low-order boundary element method at the trailing edge of a hydrofoil and its effect on the global solution", *Computers and Fluids*, Vol. 23 No. 1, pp. 63-75.

Kinnas, S., Mishima, S. and Brewer, W. (1994), "Nonlinear analysis of viscous flow around cavitating hydrofoils", *Proceedings: Twentieth Symposium on Naval Hydrodynamics*, pp. 446-65.

Kinnas, S., Pyo, S., Hsin, C-Y. and Kerwin, J. (1993), "Numerical modelling of propeller tip flows", *Proceedings: Sixth International Conference on Numerical Ship Hydrodynamics.*, pp. 531-44.

Kinnas, S., Choi, J., Lee, H. and Young, J. (2000), "Numerical cavitation tunnel", *Proceedings: NCT50, International Conference on Propeller Cavitation*, pp. 3-5.

Kinnas, S., Choi, J-K., Kakar, K. and Gu, H. (2001), "A general computational technique for the prediction of cavitation on two-stage propulsors", *Proceedings: 26th American Towing Tank Conference*, 23-24 July, Paper No. 1, pp. 1-25.

Kinnas, S., Choi, J-K., Lee, H., Young, Y., Gu, H. and Karan, K. (2002), "Prediction of cavitation performance of single/multi-component propulsors and their interaction with the hull", *Trans. SNAME*, Vol. 110, pp. 215-44.

Lee, J-T. (1987), "A potential based panel method for the analysis of marine propellers in steady flow", Doctoral dissertation, Department of Ocean Engineering, MIT.

Lee, H.S. (2002), "Modeling of developed tip vortex cavitation and unsteady wake alignment", Doctoral dissertation, Department of Civil Engineering, The University of Texas, Austin.

Lee, H. and Kinnas, S. (2001), "Modeling of unsteady blade sheet and developed tip vortex cavitation", *Proceedings: CAV 2001: Fourth International Symposium on Cavitation*, 20-23 June, California Institute of Technology, Pasadena, CA.

Lee, H. and Kinnas, S. (2003), "Fully unsteady wake alignment for propellers in non-axisymmetric flows" (in press).

Lee, C-S., Kim, Y-G. and Lee, J-T. (1992), "A potential-based panel method for the analysis of a two-dimensional super- or partially- cavitating hydrofoil", *Journal of Ship Research*, Vol. 36 No. 2, pp. 168-81.

Lemonnier, H. and Rowe, A. (1988), "Another approach in modelling cavitating flows", *Journal of Fluid Mechanics*, Vol. 195.

Matsuda, N., Kurobe, Y., Ukon, Y. and Kudo, T. (1994), "Experimental investigation into the performance of supercavitating propellers", *Papers of Ship Research Institute*, Vol. 31 No. 5.

Morino, L. and Kuo, C-C. (1974), "Subsonic potential aerodynamic for complex configurations : a general theory", *AIAA Journal*, Vol. 12 No. 2, pp. 191-7.

Mueller, A. and Kinnas, S. (1999), "Propeller sheet cavitation predictions using a panel method", *Journal of Fluids Engineering*, Vol. 121, pp. 282-8.

Riabouchinsky, D. (1926), "On some cases of two-dimensional fluid motion", *Proceedings of London Math Society*, pp. 185-94.

Rowe, A. and Blottiaux, O. (1993), "Aspects of modeling partially cavitating hydrofoils", *Journal of Ship Research*, Vol. 37 No. 1, pp. 34-48.

Russel, A. (1958), "Aerodynamics of wakes, existence of unsteady cavities", *Engineering*, Vol. 186, pp. 701-2.

Tabbara, M., Blacker, T. and Belytschko, T. (1994), "Finite element derivative recovery by moving least squares interpolants", *Computational Methods in Applied Mechanical Engineering*, Vol. 117, pp. 211-23.

Tulin, M. (1953), "Steady two-dimensional cavity flows about slender bodies", *Technical Report, 834*, DTMB.

Tulin, M. and Hsu, C. (1980), "New applications of cavity flow theory", *Proceedings: 13th Symposium on Naval Hydrodynamics*.

Uhlman, J. (1987), "The surface singularity method applied to partially cavitating hydrofoils", *Journal of Ship Research*, Vol. 31 No. 2, pp. 107-24.

Uhlman, J. (1989), "The surface singularity or boundary integral method applied to supercavitating hydrofoils", *Journal of Ship Research*, Vol. 33 No. 1, pp. 16-20.

Villat, H. (1914), "Sur la validité des solutions de certain problem d' hydrodynamique", *Journal de Mathematiques*, Vol. 6 No. 10, pp. 231-90.

Wu, T. and Wang, D. (1964), "A wake model for free-streamline flow theory. Part 2: cavity flows past obstacles of arbitrary profile", *Journal of Fluid Mechanics*, Vol. 18, pp. 65-93.

Yamaguchi, H. and Kato, H. (1983), "On application of nonlinear cavity flow theory to thick foil sections", *Proceedings: Second International Conference on Cavitation, IMechE*, pp. 167-74.

Young, Y.L. (2002), "Numerical modeling of supercavitating and surface-piercing propellers", Doctoral dissertation, Department of Civil Engineering, The University of Texas at Austin.

Young, Y. and Kinnas, S. (2001), "A BEM for the prediction of unsteady midchord face and/or back propeller cavitation", *Journal of Fluids Engineering*.

Young, Y. and Kinnas, S. (2002a), "Application of bem in the modeling of supercavitating and surface-piercing propeller flows", *Proceedings: IABEM 2002 Symposium*, pp. 28-30, May.

Young, Y. and Kinnas, S. (2002b), "A BEM technique for the modeling of supercavitating and surface-piercing propeller flows", *24th Symposium on Naval Hydrodynamics*, 8-13 July.

Young, Y. and Kinnas, S. (2003), "Numerical modeling of supercavitating propeller flows", *Journal of Ship Research*, Vol. 47, pp. 48-62.

Young, Y., Lee, H. and Kinnas, S. (2001), "PROPCAV (version 1.2) user's manual and documentation", Technical Report No. 01-4, Ocean Engineering Group, UT Austin.